

Improving the Representation and Extraction of Contact Information in Vision-based Tactile Sensors Using Continuous Marker Pattern

Mingxuan Li, *Student Member, IEEE*, Yen Hang Zhou, Tiemin Li, and Yao Jiang, *Member, IEEE*

Abstract— Tactile perception has been a hot topic of research in robotics. Robots sense the shape, material, distributed force, slip during contact, and use the multi-modal contact information to control grasping and manipulation. For vision-based tactile sensors, the contact representation and extraction determine the quality of the raw tactile information, and therefore serve a significant role in the robot perception system. This article highlights for the first time the importance of raw representation and extraction in visuotactile perception, and proposes a new multicolor CMP method for enhancing the performance of vision-based tactile sensors. Based on the principle of continuous marker pattern (CMP), the multicolor CMP method is optimized in the pattern and algorithm design. Regarding information representation, we present a new type of marker pattern based on RGB triangles and a preferred layout. In terms of information extraction, we propose a series of extraction strategies with the adaptive growing algorithm (AGA) and the spin-search algorithm (SSA) as the cores. The experiments reveal that the multicolor CMP method achieves improved precision and reliability compared to the former CMP method.

I. INTRODUCTION

The sensory system has long been an integral part of robotics. Robots interact with the external environment and receive information feedback from visual perception [1] and tactile perception [2]. Tactile sensors allow robots to acquire contact information directly, thus offering the possibility of highly reliable and adaptive robotic grasping and manipulation [3]. In recent years, different types of tactile sensors have been developed [4], [5]. Among them, vision-based tactile sensors (also called visuotactile sensors) [6], [7] are a class of sensors with the advantages of high-resolution and multi-modal perception, such as GelForce [8], GelSight [9], GelSlim [10], FingerVision [11], TacTip [12], and OmniTact [13]. These sensors use a soft elastomer to contact the objects. During contact, the deformation of the soft elastomer reflects the physical contact information and is converted into the optical signal using representation mediums. Finally, the optical signal is extracted by an image acquisition device. Contact information transformation, representation, and extraction are performed sequentially in the above process. Such sensors have been applied to geometry recognition [14], object localization [15], material identification [16], slip detection [17], and manipulation control [18], among other scenarios.

The marker pattern method, also known as the marker displacement-based method [7], is commonly used in vision-

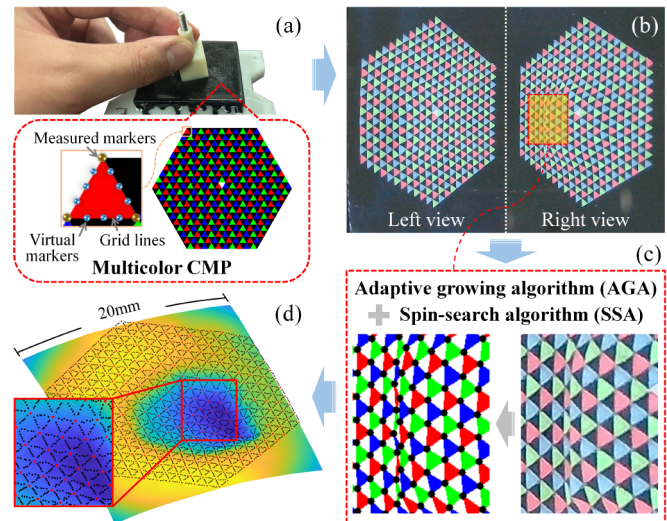


Fig. 1. (a) The multicolor CMP for high-precision contact representation. (b) Binocular tactile image of the visuotactile sensor. (c) The adaptive growing algorithm (AGA) and the spin-search algorithm (SSA) for high-reliability extraction. (d) The result of dense 3-d deformation reconstruction.

based tactile sensors to represent and extract the contact information [see Fig. 1(a)]. A marker pattern is typically printed or embedded on the surface or inside the soft elastomer to provide texture information. When the soft elastomer is deformed by force, the movement of the pattern characteristic points, also called markers, can reflect the dynamic contact deformation. Thus, the *representation* of contact information can be realized.

The *extraction* of contact information can be divided into two steps: marker recognition and marker tracking. Marker recognition identifies the markers and obtains their coordinates during deforming, while marker tracking means matching the corresponding markers in the adjacent camera frames (also known as image registration). Finally, the discrete information reflected by the markers can be transformed into a continuous field by interpolation, which serves as the basis for multimodal information reconstruction.

Current implementations of such sensors mainly focus on the design of optical paths and structures [19], [20], algorithm optimizations [21], [22], and applications like robot control strategies [23], [24]. However, few studies have focused directly on the basic function of the tactile sensor, i.e., the

*Research supported by the National Science Foundation of China under Grant 51705274, a grant from the Institute for Guo Qiang, Tsinghua University, National Training Program of Innovation and Entrepreneurship for Undergraduates under Grant 202210003017, Tsinghua University Initiative Scientific Research Program, and iCenter Star of Innovation

Program from the Fundamental Industry Training Center, Tsinghua University. M. Li, Y. H. Zhou, T. Li, and Y. Jiang are with the Institute of Manufacturing Engineering, Department of Mechanical Engineering, Tsinghua University, Beijing, China. (Corresponding author: Yao Jiang, E-mail: jiangyao@mail.tsinghua.edu.cn).

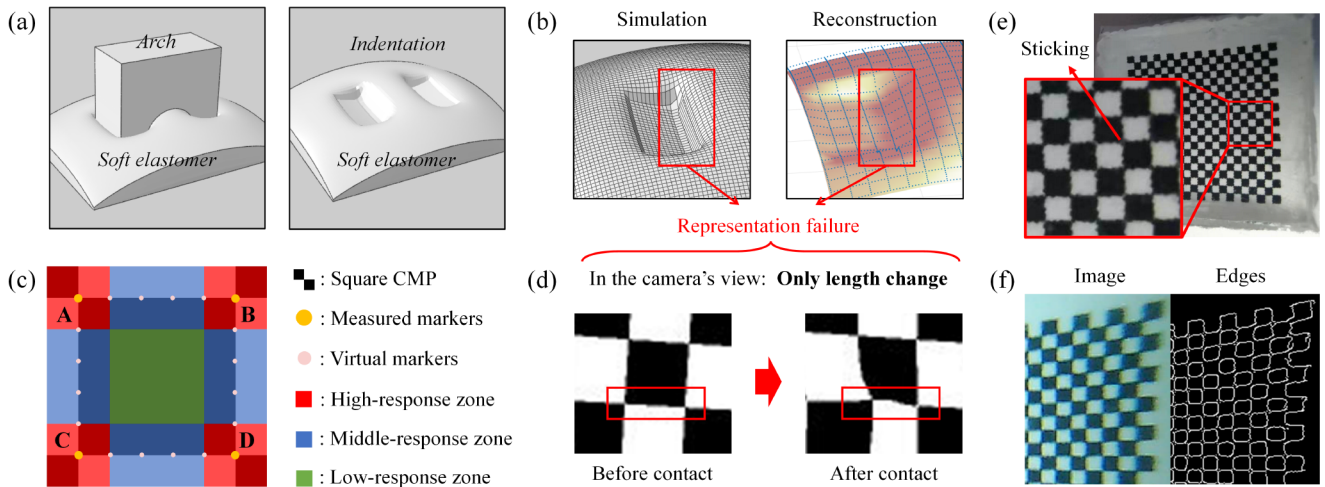


Fig. 2. Problems in the former square CMP. (a) An arch in contact with the soft elastomer. (b) Comparison between simulated and reconstructed geometry. (c) Contact response zone of the square CMP. (d) Odd angle phenomenon. (e) A remarkable sticking case. (f) Edge extraction results with sticking phenomenon.

contact information representation and extraction, which determine the quality of raw tactile information and play a decisive role in the performance of the tactile sensor. Therefore, we aim to go beyond the specific structure of sensors, directly study the mechanism of contact information representation and extraction, and provide theoretical support for the optimization and application of sensors.

Our research focuses on improving the performance of tactile sensors through the optimization of contact information representation and extraction. We previously proposed an approach for representing contact information in vision-based tactile sensors, the method of continuous marker pattern (CMP) [25]. The proposed CMP is a concept rather than a fixed implementation of marker patterns, which allows us to achieve high performance through pattern and algorithm optimization.

This article presents a new type of CMP, the multicolor CMP, and the related algorithms (AGA and SSA) to enhance the contact information representation and extraction of vision-based tactile sensors, as shown in Fig. 1. The main contributions include:

1) We propose the multicolor CMP method for contact information representation and extraction of tactile sensors and provide the corresponding algorithm.

2) Through experiments and evaluations, we verify that the proposed method can improve the precision and reliability of visuotactile sensing. Our work provides new ideas for the enhancement of vision-based tactile sensors.

II. OPTIMIZATION OBJECTIVES

In our previous work [25], the square CMP is selected as the generic CMP. It is a type of CMP with square blocks as the basic unit and a minimum of color combinations, which has the advantages of simple preparation and high versatility. However, in practice, this simple pattern has some problems in representation and extraction that need to be optimized.

A. Representation: Optimization of pattern design

The design of the marker pattern determines the feature mode of deformation visualization, thus affecting the quality of contact information representation. Here we propose two requirements to enhance the representational capabilities.

1) Precision

As shown in Fig. 2(a), we use an arch-like object in the simulation to contact a soft elastomer with the square CMP, and use the related extraction algorithm to construct the contact geometry. Fig. 2(b) shows that the contact geometry need to be reconstructed better, especially at the location of the large deformation gradient. There are two main factors:

The contact position is in the low-response zone. Imagine that a concentrated load f acts on the contact surface. The closer the load position of f is to a certain marker, the larger the three-dimensional displacement of that marker point. Therefore, we can divide the area between four adjacent measured markers into three different zones according to the contact responsive ability [see Fig. 2(c)]. The response ability reflects the local resolution. Therefore, in the case of arch contact, the reactivity and local resolution are low since the proportion of low-response areas in the contact area is large.

Singular angles exist in the representation. As shown in Fig. 2(d), when the camera is located directly above the contact surface, no significant deformation of the depressed gridline can be captured in the camera's field of view, resulting in missing reconstruction details. We refer to these angles as singular angles that can lead to representation failure. Due to the unknown camera position and light path, changing the overall angle of grid lines does not avoid this situation.

Therefore, the grid lines should be staggered at different angles to avoid concentrated distribution of low-response zones and odd orientations, thus ensuring fine representation.

2) Robustness

Due to the limitation of the preparation and the camera's image blur, the corner points of the checkerboard grid always have different degrees of sticking [see Fig. 2(e), (f)]. The sticking phenomenon can produce redundant color blocks, seriously affecting the edge extraction and corner point recognition and making the subsequent algorithm processing difficult. Such inherent deficiency seriously affects the robustness of the information representation.

The above discussion illustrate that the basic units of the pattern should be distinguishable and associated with good discriminative properties. Therefore, it is simpler to reduce the influence of the sticking through algorithms.

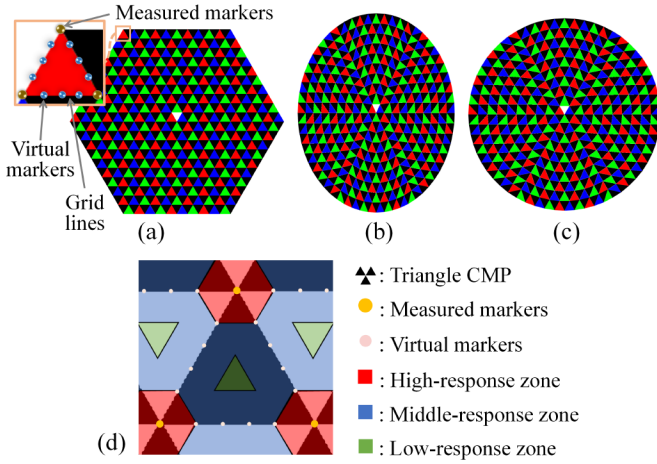


Fig. 3. Pattern design of the multicolor CMP method. (a) Honeycomb. (b) Elliptical. (c) Round. (d) Contact response zone of the multicolor CMP.

B. Extraction: Optimization of algorithm design

The algorithm design determines the contact information extraction. The optimization should focus on the accurate and complete acquisition of the contact information to ensure the extraction process's reliability in general and specific cases.

1) Recognition accuracy

Under the same condition, the recognition accuracy of algorithm determines the quality of the acquired contact information. The optimized algorithm should be able to guarantee sub-pixel recognition accuracy.

2) Recognition reliability

Different interference factors, such as background colors and uneven external lighting, can lead to recognition errors. The optimized algorithm should minimize the range of feature recognition to exclude interference and ensure reliability.

3) Tracking reliability

The contact information can only be captured correctly if the displacement of the marker during deformation can be tracked. If the algorithm's reliability cannot be guaranteed, the potential of rigid tracking [25] in CMP could be difficult to manifest. Thus, optimizing the tracking strategy is necessary.

4) Special Cases

In practice, when the contact load is large (such as large tangential force), the pattern edge could be difficult to visual distinguish since it is squeezed into a line or out of the effective camera's view. In addition, interference from illumination and material defects in the soft elastomer may interfere with feature recognition, resulting in a loss of local information.

Therefore, we suggest the seeded region growing method to the original contour-based algorithm to improve recognition accuracy and reliability. Besides, we introduce a mechanism of reference marker arrangement to the rigid tracking-based algorithm, which allows us to sort the markers more robustly and even handle the common marker omissions.

III. MULTICOLOR CONTINUOUS MARKER PATTERN

A. Pattern design

Based on the three basic principles of CMP [25], we propose a new set of designs (the multicolor CMP), as shown in Fig. 3.

1) Colored units

The basic unit of the multicolor CMP is colored triangles [see Fig. 3]. To address the limitations caused by sticking, the

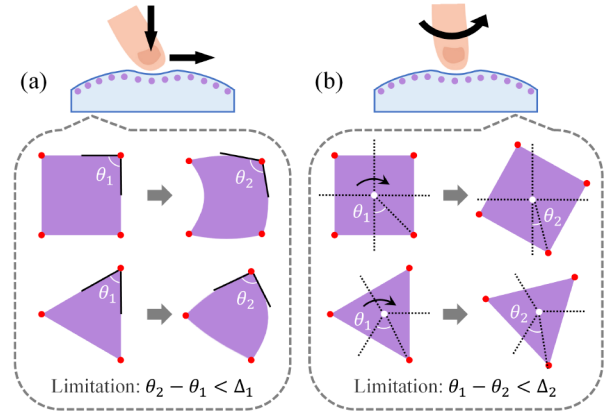


Fig. 4. The influence of contact deformation on marker patterns (a) Contact mode: Pressing. (b) Contact mode: Twisting.

adjacent basic units are selected as red, green, and blue. Through this design, the difference in color gamut can be used to distinguish pixels belonging to different units, thus ensuring the precision of contour recognition. Besides, pattern units of the same color are separated in space. They can be more easily distinguished under different deformation and illumination modes than black-and-white units, allowing for high reliability in recognition when the marker patterns are pulled or squeezed.

The black triangles are used to accentuate the light-color marker pattern and suppress the scattered light, which should be ignored during the extraction process since the RGB triangles already contain the grid lines. A triangle in the center of the marker pattern is set to white, which provides the starting point reference in the tracking algorithm.

2) Triangular units

The triangular pattern (so-called Deltile) is one of the three regular tilings in the Euclidean plane. Compared to the square pattern, such design has higher precision and resistance to contact deformation as follows.

By comparing Fig. 2(c) and Fig. 3(d), it can be seen that the triangular pattern has a more compact feature arrangement than the square pattern. Such a feature disperses the low-response zones into different units to avoid a concentrated distribution. Each set of hexagon contains six grid-lines with different angles. Thus, even if one grid line is at an odd angle, the other five grid lines still work properly. Besides, the triangular pattern has been shown to have accuracy advantages in providing localization references. Ha *et al.* demonstrated that the richer constraint information provided by this pattern could contribute to accurate localization [26]. According to Bommes *et al.* [27], triangles are structurally flat and convex, and can be described qualitatively using the deviation from an equilateral triangle and the largest angle. These features make it more suitable as a 3D calibration primitive.

The resistance to contact deformation can be quantified as the size of the internal corners of the pattern. As shown in Fig. 4, the two main contact modes, pressing and twisting, respectively affect the shape change and rotation around the center of the marker unit. When the shape change is greater than 180° , the corner feature fails to be recognized; When a corner of the unit is rotated to cross the mid-line between adjacent corner points in the original pattern, the relative orientation change will cause the corner feature to be tracked incorrectly. For a regular n -sided shape, the threshold values for the deviation angle Δ_1 and rotation angle Δ_2 are

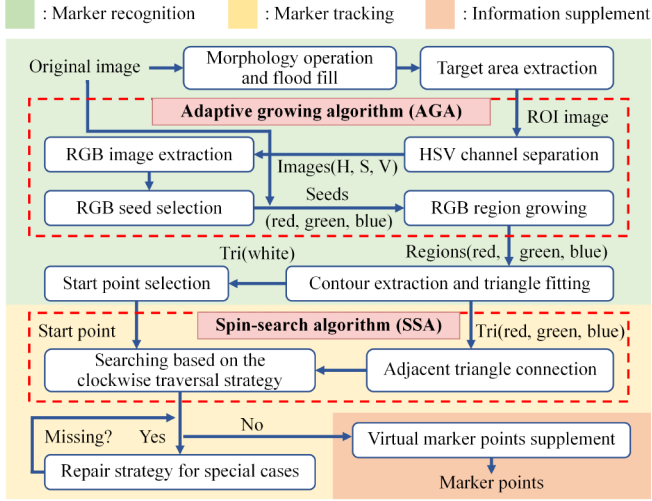


Fig. 5. Algorithm design of the multicolor CMP method, with the adaptive recognition algorithm (ARA) and spin-search algorithm (SSA) as the cores.

$$\Delta_1 = 180^\circ - \frac{n-2}{n} \cdot 180^\circ = \frac{360^\circ}{n}, \quad (1)$$

$$\Delta_2 = 90^\circ - \frac{n-2}{2n} \cdot 180^\circ = \frac{180^\circ}{n}. \quad (2)$$

When the angles are less than the related thresholds, the corner can still be recognized and tracked. From the above analysis, the larger Δ_1 and Δ_2 , the higher the deformation that can be tolerated. Therefore, selecting a triangular shape with the minimum n can help improve reliability in visuotactile sensing.

3) Arrangement

The multicolor CMP can be arranged like a honeycomb [see Fig. 3(a)], which is suitable for flatter contact surfaces. We can also use non-positive hexagonal shapes to make the mark pattern oval or circular [see Fig. 3(b), (c)]. This arrangement is more compact and can maximize the utilization of the pattern's amplitude. The algorithms corresponding to the three styles are basically the same. In addition, we propose to let the hexagons be arranged in circle layers from the center outward. In this arrangement, the marker units are set in a good geometric regularity, which facilitates the design of inside-out numbering algorithms and correction algorithms for special cases.

B. Algorithm design

The information extraction algorithm of multicolor CMP includes marker recognition, marker tracking, and information supplementation. The algorithm process is shown in Fig. 5.

1) Marker recognition

First, the RGB marker units should be recognized from the redundant image information. Inspired by the classical seeded region growing method (SRG) [28] and its application in the segmentation of color images [29], we propose the *adaptive growing algorithm (AGA)* to avoid the sticking phenomenon and improve the recognition reliability [see Fig. 6].

Target area extraction. By the water diffusion algorithm and morphological operation, we extract the target zone and reduce the influence of the background by removing the pixels that do not belong to the marker pattern, as shown in Fig. 6(b).

HSV color segmentation. We convert the image to the HSV color space format, use a mask to divide the area in the Hue channel to filter the color, and finally differentiate the RGB

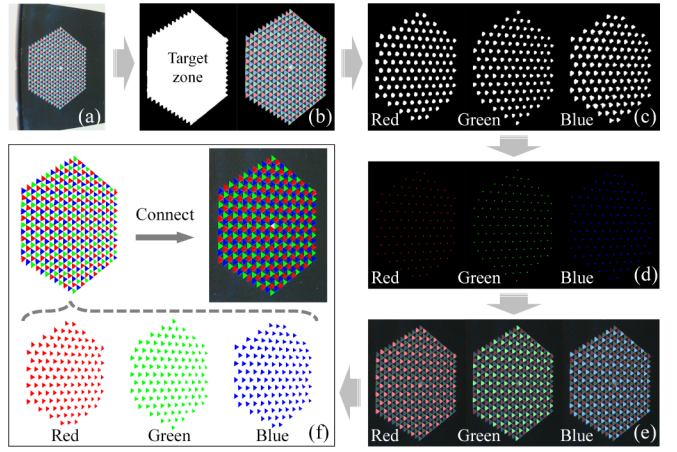


Fig. 6. Marker recognition based on the adaptive growing algorithm (AGA). (a) Original image. (b) Target area extraction. (c) HSV color segmentation. (d) Seed selection. (e) Region growing. (f) Triangle fitting and connection.

contours [see Fig. 6(c)]. Since the color distortion caused by illumination mainly affects the saturation and brightness, the color segmentation based on the Hue channel of HSV color space has good integrity and correctness.

RGB seed selection. After removing the small fragments of noise and clutter, the geometric center of each domain is selected as the RGB seed for region growing [see Fig. 6(d)].

RGB region growing. Let S_1, S_2, \dots, S_i denote the initial seeds, and A_i denotes the growing region corresponding to S_i . Let the average color of pixels in A_i be $(\bar{H}^i, \bar{V}^i, \bar{S}^i)$. In this step, we form the region A_i based on the color difference, taking S_i as the center and growing from inside to outside.

Let the pixel P adjoin with A_i (consider 4-neighbors) and its color denotes (H_p^i, V_p^i, S_p^i) . The color difference between P and A_i is calculated as the relative Euclidean distance

$$d_p^i = \frac{\sqrt{(H_p^i - \bar{H}^i)^2 + (V_p^i - \bar{V}^i)^2 + (S_p^i - \bar{S}^i)^2}}{\sqrt{H_p^i \times \bar{H}^i + V_p^i \times \bar{V}^i + S_p^i \times \bar{S}^i}}. \quad (3)$$

From our experiment, 0.15 is selected as the threshold. If d_p^i is less than this threshold, P is considered to be similar in color and added to A_i . Initially, the region A_i consists of S_i only. By repeating the above process, the S_i region continues to grow from inside to outside until no pixel has the Euclidean distance less than the threshold.

Finally, each RGB seed generates a region corresponding to a triangle unit of its color [see Fig. 6(e)]. This strategy can constantly update the benchmark of Euclidean distance during the process and, therefore, have high adaptability and reliability. Besides, the “growing from the inside out” feature also ensures the structural accuracy of the extracted region.

Triangle fitting. For the different RGB regions, we preserve the contours that belong to the RGB triangles according to the area, perimeter, and other conditions. We extract three corners from each sub-contour to form a topological triangle, i.e., a triangle connection relation stored as a point-set [see Fig. 6(f)].

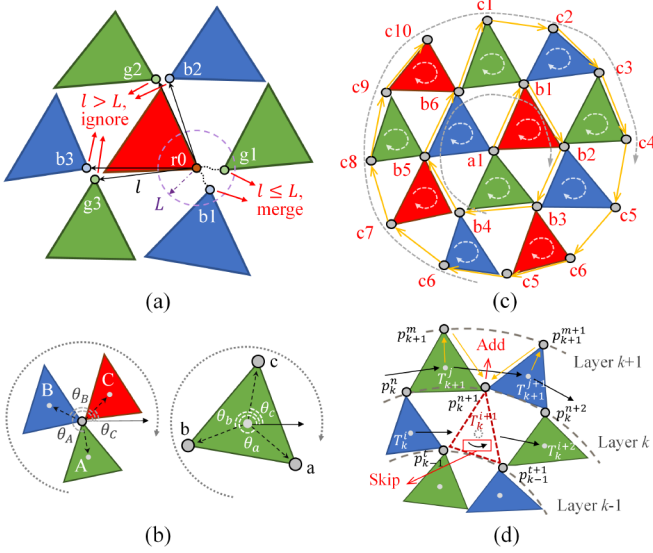


Fig. 7. Marker tracking based on the spin-search algorithm (SSA). (a) Adjacent triangle connection. (b) The clockwise traversal strategy. (c) The implementation of SSA. (d) Repair strategy in case of small omission.

2) Marker tracking

Marker tracking is achieved by matching markers with the same serial number in different camera frames according to the connection relationship between adjacent tags. Based on the analysis in Section II, we propose the *spin-search algorithm (SSA)* to achieve rigid tracking based on the shape and the arrangement of the basic cells [see Fig. 7].

Adjacent triangle connection. As shown in Fig. 7(a), the connection of the red triangle at corner r_0 is introduced as an example. Since each corner is at most adjacent to a green triangle and a blue triangle, it is practicable to find the corner points connected to r_0 by simply searching within the green and blue triangles adjacent to the red triangle, respectively. Let the vector pointing from the corner r_0 to g_i denotes $\vec{l}_{g_i}^{r_0}$, and the corner points that need to be merged with r_0 form the point-set

$$S_{\text{merge}}^{r_0} = \{g_1, b_1\}, \quad (4)$$

and the remaining corner points form $S_{\text{other}}^{r_0}$. The minimum distance threshold L^{r_0} is preset. Under different deformations, L^{r_0} satisfies the function

$$\begin{cases} |\vec{l}_{g_i}^{r_0}| \leq L^{r_0}, & g_i \in S_{\text{merge}}^{r_0} \\ |\vec{l}_{g_i}^{r_0}| > L^{r_0}, & g_i \in S_{\text{other}}^{r_0} \end{cases}. \quad (5)$$

Therefore, it is possible to determine whether to perform the association operation on the corner r_0 and corner g_i by judging the distance relationship. The same procedure is performed for the blue and green triangles, except that the already connected corner points are ignored to reduce the computation time. Finally, the average coordinate values of r_0 , g_1 , and b_1 are taken as the coordinate values of the merged corner points. The above process constructs a topological connectivity graph of markers [see Fig. 6(f)], and effectively avoid the connection errors by the differentiation between the basic units.

Search based on the spin-search algorithm. The spin-search algorithm requires the corner points to be traversed in the same direction (like clockwise). The following strategy implements

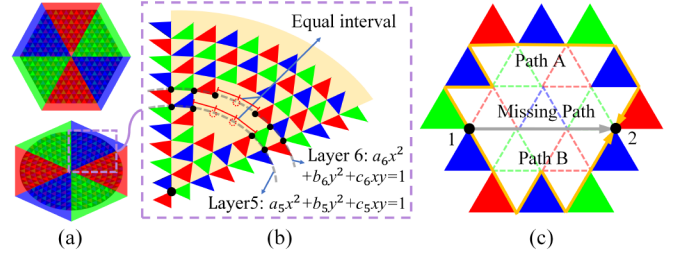


Fig. 8. Repair strategy in case of heavy omission. (a), (b) Fitting based on the quadratic form. (c) Different paths from point 1 to point 2.

SSA: When traversing the three corners of a triangle, each corner is searched clockwise according to its azimuth relative to the center point of the triangle; when traversing the three triangles around a corner, each triangle is searched clockwise according to the azimuth of its center point [see Fig. 7(b)].

For the previously mentioned white triangle, its bottom corner is used as the starting point of the traversal process. From that point, we traverse each marker from the inside out in a hierarchical manner [see Fig. 7(c)]. The traversal process is divided into two parts: 1) traversal within the same layer, and 2) traversal from the inner layer to the outer layer. For example, the path from b_1 to c_4 implemented by the SSA-based traversal algorithm in Fig. 7(c) can be expressed as $\{b_1, b_2, b_3, b_4, b_5, b_6, c_1, c_2, c_3, c_4\}$.

Repair strategy for omission cases. There are two main types of omission cases caused by interference: the loss of valid details at the edge of the pattern and the loss of valid information inside. For the first case, since the search order of SSA is inside-out, when the feature points on the outer side are lost, the affected outer layers can be discarded to ensure the feature points on the inner layers still achieve representation.

For the latter case, if only one or two triangles are missing along with their corner points (mild omission), we supplement the position information of the lost markers using the triangles adjacent to them [see Fig. 7(d)]. Let the missing triangle be T_k^{i+1} between Layer $k-1$ and Layer k , and the missing marker denotes p_k^{n+1} . It is first necessary to find the triangle T_k^j and triangle T_k^{j+1} , which satisfy the function

$$\begin{cases} T_k^i \cap T_k^j = p_k^n \\ T_k^{i+2} \cap T_k^{j+1} = p_k^n \\ T_k^j \cap T_k^{j+1} = p_k^{n+1} \end{cases} \quad (6)$$

Thus, the next corner of corner p_k^m in triangle T_k^j and the previous corner of corner p_k^{m+1} in triangle T_k^{j+1} are obtained. Besides, these two points are theoretically the same corner. Considering the error in the actual detection, the average of the two coordinates is taken to calculate the coordinate of p_k^{n+1} .

In addition, if the omission is heavy, the missing markers can be approximately repaired by using the geometric regularity of the arrangement. We divide the marker pattern into six areas [see Fig. 8(a)]. For the honeycomb and elliptical (round) CMP, the markers of the same layer in each area are arranged in a line and a circular arc. It means that we can use the quadratic fitting and equidistant interpolation to get the missing marker based on the same-layer ones [see Fig. 8(b)].

Since the marker pattern's shape is changing, the repairing process has low confidence and will fail when all the markers

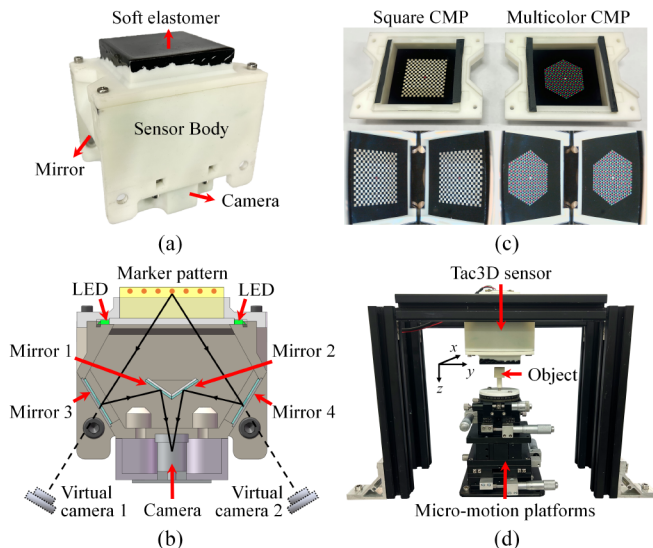


Fig. 9. Experimental equipment. (a) Tac3D 3.0 sensor. (b) Virtual binocular vision principle [30]. (c) The detachable soft elastomers with the square CMP and multicolor CMP and their images in the camera view. (d) Experimental platform for evaluations.

of the same layer are lost. Besides, the basis of the above repair strategy is the rigid attribute of the multiple CMP. Since all the basic units are physically connected, we can always find other paths to bypass the damaged area and set the serial numbers of all the non-lost marker points. Fig. 8(c) shows the paths from point 1 to point 2. Thus, for a certain marker, we can always use the same-layer markers to repair it (unless the whole layer is missing), which already cope with the actual application.

3) Information supplement

Our previous work [25] shows that virtual marker points can be obtained by discretizing ideal grid lines to supplement two-dimensional information. Since each set of virtual marker points is determined by the gridline between two adjacent measured marker points, the orderly numbering and rigid tracking of virtual marker points can be achieved using the already numbered measured markers. The supplement of virtual marker points can balance the algorithm's efficiency and the comprehensiveness of the information representation.

IV. EVALUATION EXPERIMENTS

In this section, we developed two sensor prototypes with the multicolor CMP and the square CMP, respectively. We focus on the relative performance comparison of these two methods rather than the sensor as a whole.

A. Experimental equipment and setup

Based on the previous work [30], we designed the Tac3D 3.0 sensor as the experimental prototype [see Fig. 9(a)]. Its body was made by 3D printing, and the soft elastomer, camera, LED light source, and lens were all fixed in the sensor housing. Tac3D 3.0 adopted the principle of virtual binocular vision as shown in Fig. 9(b). It could use only one camera to realize binocular stereo vision, so as to ensure binocular synchronous triggering in the experiment.

Besides, we adopted a new preparation process for the soft elastomers, which were made multi-layer, including the base layer, the marker pattern layer, and the protective layer. The core of the new process is to carve holes on the cast elastomer

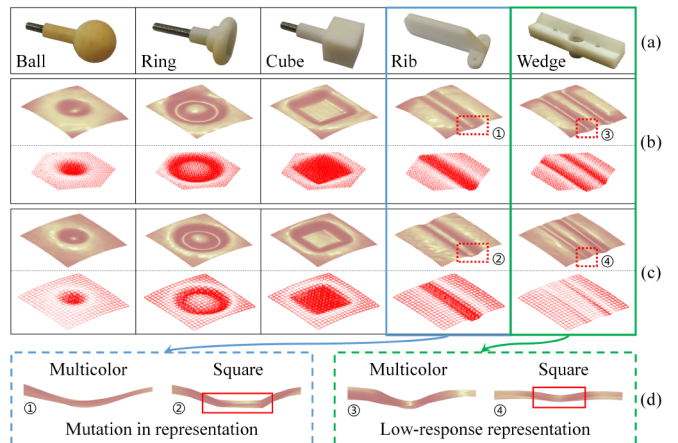


Fig. 10. Comparison of reconstructed contact deformation. (a) Test objects. (b) The reconstruction of the square CMP. (c) The reconstruction of the multicolor CMP. Red arrows represent the displacement of marker points. (d) Comparison of sharp contact characteristics (amplification of the side view).

using laser and fill them with colored silicone, ensuring that the colored pattern can have clear texture and can be deformed with the elastomer. We made two elastomers with the square CMP and the multicolor CMP, respectively [see Fig. 9(c)]. They are designed to be detachable and can be easily replaced in experiments. Since the main part of the sensor remained unchanged during the replacement process, we could focus on the effect of the patterns on measurement only and compare the performance of them through evaluation experiments. The edge length of each basic unit in the two modes is set equal to 1.5mm to ensure the fairness of the comparison.

All experiments were performed on the test platform shown in Fig. 9(d). Using a combined micro-motion platform, we could replace different shapes of test objects and control the contact (including three-axis force and one-axis torque) in different positions and orientations. Since our purpose is to compare the performance of the two CMP methods rather than the performance of the sensor as a whole, this article only used the raw deformation as the basis for the evaluation.

Related algorithms were running on a laptop (i7-12700H processor at 2.30 GHz, 14 cores, and 16.0 GB of RAM) and implemented by C++ OpenCV. In real-time practice without optimization, the processing frequencies for the two methods achieved 20 Hz (the square CMP) and 16 Hz (the multicolor CMP). The main reason for the speed limit lay in the large amount of marker points (nearly 5000 points including virtual marker points). For the task of dense 3D displacement field reconstruction, such frame rate could meet the requirements.

B. Precision Evaluation

Precision is mainly expressed in the degree of conformity between the measured results and the actual values. We selected five different objects to contact the soft elastomers by squeezing them for 2mm in the normal direction [see Fig. 10(a)]. The purpose of this experiment was to qualitatively compare the representation of two CMP methods for the same contact deformation. As shown in Fig. 10(b) and 10(c), the 3D morphologies and displacement fields were reconstructed by the two CMP patterns, respectively. When the contact surface was relatively smooth (e.g., using a ball or a ring), the deformation reconstructions of the two methods were not obviously different. However, when the contact surface was

TABLE I. RELIABILITY TEST RESULTS OF TWO CMP METHODS

The CMP method	Contact mode 1		Contact mode 2		Contact mode 3	
	Successful	Failed	Successful	Failed	Successful	Failed
The square CMP	7	3	6	4	6	4
The multicolor CMP	9	1	7	3	10	NA
The multicolor CMP with repair strategies	10	NA	10	NA	10	NA

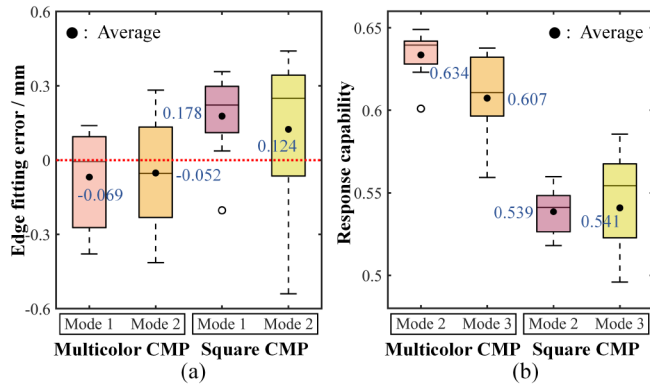


Fig. 11. Comparison of the Edge fitting error and response capability comparison. (a) Edge fitting error. (b) Response capability.

sharp (e.g., using a rib or a wedged block), the multicolor CMP could avoid the sharp mutation and distortion caused by the concentrated distribution of low-response zones, and thus presenting clearer edges with high resolution. [see Fig. 10(d)].

We further defined the edge fitting error and response capability to judge the measurement refinement of both methods quantitatively. A cube with a side length of 15mm was chosen as the test object for contact with the soft elastomer. On the two elastomers, ten same positions were selected at equal intervals (4mm in x - or y -directions). We used the micro-motion platforms for each position to control two contact modes: 1) Press to a depth of 1 mm (z -direction). 2) Press to a depth of 1 mm, then shear 1 mm tangential (y -direction). The markers in the contact area should have corresponding z - or y -direction displacement. Considering the contact slip, we selected the markers that moved more than half of the maximum displacement to join an edge-point set. We further fitted the maximum circumscribed square of the point set, which was the contact edge that the marker pattern could represent. The closer the square's side length obtained by fitting was to 15 mm, the more accurate the CMP was in characterizing the sharp characteristics under current contact. The error distribution under different conditions are shown in Fig. 11 (a). The results reveal that the multicolor CMP can obtain more accurate measurement and the edge fitting error is reduced by 61.2% and 58.1%, respectively.

For shear contact, although the elasticity of the contact part could hinder the movement of markers in the horizontal direction, the markers closer to the contact edge still had greater displacement. Under the same setting as the above experiment, we added a group of contact modes: 3) Press to a depth of 1 mm, then shear 1mm tangential (x -direction). We obtained the edge-point set of the second and third contact modes and calculated the average displacement of the points in the corresponding shear direction, as shown in Fig. 11 (b).

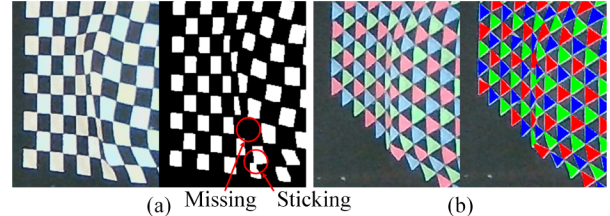


Fig. 12. Comparison of original recognition results. (a) The recognition result of the square CMP. (b) The recognition result of the multicolor CMP.

The response capacity is defined as the ratio of the average value to the shear amount (as 1mm). The multicolor CMP's responsiveness in x - and y -directions has been improved by 17.6% and 12.2%, respectively. It shows that the multicolor CMP has reduced the proportion of markers at the contact edge distributed to be in the low response area.

The above experiments show that the multicolor CMP method has a higher precision in local and global than the square CMP method. On the one hand, the multicolor CMP has higher compactness under the same basic unit length (i.e., the spacing of markers) and avoids the concentrated distribution of low response areas, thus avoiding the loss of sharp contact characteristics. On the other hand, the multicolor CMP can solve the singular angle problem, thus improving the deformation reconstruction at the contact position.

C. Reliability Evaluation

In this subsection, different extreme loading conditions were selected to compare the reliability performance of the two methods. We put a test ball with a radius of 20mm in contact with the soft elastomers at ten groups of sampling positions, which were equally spaced. Three types of contact modes were applied on each sampling position: 1) Press to a depth of 2 mm, then twist 30 degrees clockwise. 2) Press to a depth of 2 mm, then shear 1.5 mm tangential (x -direction). 3) Press to a depth of 2 mm, then shear 1.5 mm tangential (y -direction). For these two different CMP methods, the test results were classified as "successful" and "failed", and recorded separately as shown in Table I].

The results show that the success rate of the multicolor CMP method is higher than that of the square CMP method. When the soft elastomer was deformed by forces, the basic units in the marker pattern would be squeezed or stretched. Fig. 12(a), (b) show a typical recognition result of the two methods under the same contact position and condition. While the square CMP could get stuck during contact and caused a loss of information in multiple contiguous units, the multicolor CMP was able to distinguish the basic units close to each other through color differences, thus avoiding these situations. Besides, Table I also reveals the effect of the newly introduced repair strategies in the multicolor CMP. Since the missing

information was all limited to single basic units, the CMP with repair strategy still obtained acceptable results for all tests.

In addition, note that the failure rates of the two CMP methods are relatively close for the second contact mode. The reason is that the x -direction shearing would make the markers in the contact area far away from one of the visual fields in the virtual binocular camera, thus improving the difficulty of recognition and tracking. Such results mean that in addition to the design of the pattern and algorithm, the optical system can also affect the measurement results. It inspires us to improve the contact representation and extraction by optimizing the imaging process in future work.

The above experiments show that the multicolor CMP method results in higher reliability. Using the RGB basic units and the AGA method can improve recognition accuracy, and the SSA method can make reliable repair strategies possible. The algorithm used for the multicolor CMP can also be modified to adapt to the square CMP and is expected to improve its reliability in representation and extraction of contact information.

V. CONCLUSION

Representation and extraction of contact information play a decisive role in the quality of raw information for robotic tactile perception. This article proposes the multicolor CMP method for enhancing tactile sensing elements' performance, especially reliability and precision. Our research starts from the optimization objectives of the CMP method and works on pattern design and algorithm design. Experimental results demonstrate that compared with the former square CMP method, the multicolor CMP method can achieve higher precision and reliability under the same hardware conditions.

In future work, we will explore the possibility of combining marker pattern methods with other related methods. For example, we attempt to combine the CMP method with other methods of representation and extraction to achieve super-resolution contact distribution force measurements. In addition, we are exploring the optimization of the preparation process of the sensor's optical system and the marker layer of the soft base component, aiming to provide the quality of the original contact information. We also plan to explore how learning-based techniques can further exploit the potential of the multicolor CMP method. These efforts will help extend the proposed approach to practical applications.

REFERENCES

- [1] A. Billard and D. Kragic, "Trends and challenges in robot manipulation," *Science*, vol. 364, no. 6446, 2019.
- [2] R. Dahiya, G. Metta, M. Valle, and G. Sandini, "Tactile sensing: From humans to humanoid," *IEEE Trans. Robot.*, vol. 26, no. 1, pp. 1–20, Feb. 2010.
- [3] R. Calandra, A. Owens, M. Upadhyaya *et al.*, "The feeling of success: Does touch sensing help predict grasp outcomes," in *Proc. Conf. Robot Learn.*, 2017, pp. 1–10.
- [4] C. Chi, X. Sun, N. Xue, T. Li, and C. Liu, "Recent progress in technologies for tactile sensors," *Sensors*, vol. 18, no. 4, 2018.
- [5] T. D. Nguyen and J. S. Lee, "Recent development of flexible tactile sensors and their applications," *Sensors*, vol. 22, no. 1, 2021.
- [6] Alexander C. Abad and A. Ranasinghe, "Visuotactile sensors with emphasis on GelSight sensor: A review," *IEEE Sensors J.*, vol. 20, no. 14, pp. 7628–7638, Jul. 2020.
- [7] M. Li, L. Zhang, T. Li, and Y. Jiang, "Marker displacement method used in vision-based tactile sensors—from 2D to 3D: A review," *IEEE Sensors J.*, vol. 23, no. 8, pp. 8042–8059, Apr. 2023.
- [8] K. Sato, K. Kamiyama, N. Kawakami, and S. Tachi, "Finger-shaped GelForce: Sensor for measuring surface traction fields for robotic hand," *IEEE Trans. Haptics*, vol. 3, no. 1, pp. 37–47, Jan.–Mar. 2010.
- [9] W. Yuan, S. Dong, and E. H. Adelson, "GelSight: High-resolution robot tactile sensors for estimating geometry and force," *Sensors*, vol. 17, no. 12, 2017, Art. no. 2762.
- [10] E. Donlon, S. Dong, M. Liu, J. Li, E. Adelson, and A. Rodriguez, "GelSlim: A high-resolution compact robust and calibrated tactile-sensing finger," in *Proc. IEEE/RSSJ Int. Conf. Intell. Robots Syst.*, Oct. 2018, pp. 1927–1934.
- [11] A. Yamaguchi and C. G. Atkeson, "Tactile behaviors with the vision-based tactile sensor FingerVision," *Int. J. Hum. Robot.*, vol. 16, no. 03, Jun. 2019.
- [12] N. Lepora, "Soft biomimetic optical tactile sensing with the TacTip: A review," *IEEE Sensors J.*, vol. 21, no. 19, pp. 21131–21143, Oct. 2021.
- [13] A. Padmanabha *et al.*, "OmniTact: A multi-directional high-resolution touch sensor," in *Proc. IEEE Int. Conf. Robot. Automat.*, 2020, pp. 618–624.
- [14] Y. Yang, X. Wang, Z. Zhou *et al.*, "An enhanced FingerVision for contact spatial surface sensing," *IEEE Sensors J.*, vol. 21, no. 15, pp. 16492–16502, Aug. 2021.
- [15] S. Cui, R. Wang, J. Hu *et al.*, "In-hand object localization using a novel high-resolution visuotactile sensor," *IEEE Trans. Ind. Electron.*, vol. 69, no. 6, pp. 6015–6025, Jun. 2021.
- [16] B. Ward-Cherrier, N. Pestell, and N. F. Lepora, "Neurotac: A neuromorphic optical tactile sensor applied to texture recognition," in *Proc. IEEE Int. Conf. Robot. Autom.*, May, 2020, pp. 2654–2660.
- [17] R. Sui, L. Zhang, T. Li, and Y. Jiang, "Incipient slip detection method with vision-based tactile sensor based on distribution force and deformation," *IEEE Sensors J.*, vol. 18, no. 22, pp. 25973–25985, Oct. 2021.
- [18] S. Tian *et al.*, "Manipulation by feel: Touch-based control with deep predictive models," in *Proc. IEEE Int. Conf. Robot. Autom.*, 2019, pp. 818–824.
- [19] I. Taylor, S. Dong, and A. Rodriguez, "GelSlim3.0: High-resolution measurement of shape force and slip in a compact tactile-sensing finger," in *Proc. IEEE Int. Conf. Robot. Autom.*, 2022, pp. 10781–10787.
- [20] H. Sun, K. J. Kuchenbecker, and G. Martius, "A soft thumb-sized vision-based sensor with accurate all-round force perception," *Nature Mach. Intell.*, vol. 4, no. 2, pp. 135–145, Feb. 2022.
- [21] L. V. Duong and V. A. Ho, "Large-scale vision-based tactile sensing for robot links: Design, modeling, and evaluation," *IEEE Trans. Robot.*, vol. 37, no. 2, pp. 390–403, Apr. 2021.
- [22] Y. Zhang, Z. Kan, Y. Yang, Y. A. Tse, and M. Y. Wang, "Effective estimation of contact force and torque for vision-based tactile sensors with helmholtz-hodge decomposition," *IEEE Robot. Automat. Lett.*, vol. 4, no. 4, pp. 4094–4101, Oct. 2019.
- [23] C. Wang, S. Wang, B. Romero, F. Veiga, and E. Adelson, "Swingbot: Learning physical features from in-hand tactile exploration for dynamic swing-up manipulation," in *Proc. IEEE/RSSJ Int. Conf. Intell. Robots Syst.*, 2020, pp. 5633–5640.
- [24] C. Pang *et al.*, "Viko: An adaptive gecko gripper with vision-based tactile sensor," in *Proc. IEEE Int. Conf. Robot. Autom.*, 2021, pp. 736–742.
- [25] M. Li, L. Zhang, T. Li, and Y. Jiang, "Continuous marker patterns for representing contact information in vision-based tactile sensor: Principle, algorithm, and verification," *IEEE Trans. Instrum. Meas.*, vol. 71, pp. 1–12, 2022, Art no. 5018212.
- [26] H. Ha *et al.*, "Deltille grids for geometric camera calibration," in *Proc. IEEE Int. Conf. Comput. Vis. (ICCV)*, 2017, pp. 5344–5352.
- [27] D. Bommers *et al.*, "State of the art in quad meshing," in *Proc. 33rd Annu. Conf. Eur. Assoc. Comput. Graph. (Eurographics)*, 2012.
- [28] R. Adams and L. Bischof, "Seeded region growing," *IEEE Trans. Pattern Anal. Mach. Intell.*, vol. 16, no. 6, pp. 641–647, Jun. 1994.
- [29] F. Y. Shih and S. Cheng, "Automatic seeded region growing for color image segmentation," *Image Vis. Comput.*, vol. 23, no. 10, pp. 877–886, Sep. 2005.
- [30] L. Zhang, Y. Wang, and Y. Jiang, "Tac3D: A novel vision-based tactile sensor for measuring force distribution and estimating friction coefficient distribution," Feb. 2022. *arXiv preprint arXiv: 2202.06211*.